Defense Technical Information Center Compilation Part Notice

ADP011113

TITLE: Buffet Active Control - Experimental and Numerical Results

DISTRIBUTION: Approved for public release, distribution unlimited

This paper is part of the following report:

TITLE: Active Control Technology for Enhanced Performance Operational Capabilities of Military Aircraft, Land Vehicles and Sea Vehicles [Technologies des systemes a commandes actives pour l'amelioration des performances operationnelles des aeronefs militaires, des vehicules terrestres et des vehicules maritimes]

To order the complete compilation report, use: ADA395700

The component part is provided here to allow users access to individually authored sections of proceedings, annals, symposia, etc. However, the component should be considered within the context of the overall compilation report and not as a stand-alone technical report.

The following component part numbers comprise the compilation report:
ADP011101 thru ADP011178

Buffet Active Control - Experimental and Numerical Results

C. Despré[1], D. Caruana[1], A. Mignosi[1], O. Reberga[1], M. Corrège[2],
H. Gassot[3], J.C. Le Balleur[3], P. Girodroux-Lavigne[3]

[1,2] ONERA, 2 av. Edouard Belin, 31400 Toulouse, France
[3] ONERA, 29 avenue de la Division Leclerc, 92322 Chatillon, France

Abstract: The study aims are the active control of transonic buffet over airfoils and wings. A new moving device at the trailing-edge, a so-called "Trailing Edge Deflector" (TED) designed at ONERA, is used to decrease the buffet instabilities.
This study is limited to buffet phenomenon on upper surface of a stiff 2D airfoil in transonic flow.
Experimental and numerical results allow to better understand the phenomena and to validate the efficiency of the TED.
The TED can be moved sequentially to a static position, or better be driven by dynamic servo-motions. A selected static position increases aerodynamic performances for high lift coefficient and delays the buffet onset vs. lift. A preferable TED active control law, coupled with measured flow signals, allows to greatly reduce the aerodynamic instabilities.
The time-consistent strong viscous-inviscid interaction approach VIS15, developed previously for computing buffet or unsteady separated flows over airfoils, gives access to a direct time-accurate simulation of the active buffet control by TED servo-command, both in open-loop control, and in the closed-loop servo-command driven by the computed self-induced signals of buffet.

Key words: *Unsteady flow, buffet, buffet control, two-dimensional flow, shock-wave interaction, flow separation, numerical method, strong interaction, viscous-inviscid interaction, active control, control law, closed-loop control, open-loop control.*

List of Symbols

c	airfoil chord, $c = 200$ mm
x	longitudinal coordinate
z	vertical coordinate
M	Mach number
U	free-stream velocity
T	temperature
P	pressure
C_p	pressure coefficient
$Re_{c,o}$	Reynolds number
ρ	density
t	time
f, f_o	frequency, natural buffet frequency
ϕ	phase
Xsh	shock wave position
α	angle of attack (degrees)
δ	angle of deflector (degrees)
δ_{mean}	static position of the deflector
A	amplification of the control law
τ	time delay of the control law

Subscripts

$(.)_o$	free stream value
$(.)_t$	total value
$(.)_{def}$	deflector value
$(.)_{mean}$	mean value
$|.|$	amplitude function for fluctuations

1. Introduction

Buffeting is characterized by structure vibrations induced by aerodynamic excitations. The buffeting phenomenon can exist on different parts of the flows around vehicles. It can appear on aircraft, rockets, turbomachine stages... In this paper, the study is focused on the upper surface of a wing in a transonic flow.

The shock wave/turbulent boundary layer interaction and flow separations induce flow instabilities, named buffet. It results in pressure fluctuations on the wing, that create unsteady loads which can cause structure vibrations on its eigen modes. The buffet loads may cause fatigue problems. In addition, maneuverability and handling qualities are often degraded.

The buffet phenomenon appears when the Mach number or the angle of attack of the aircraft increases. The flight envelope is limited by this phenomenon.

Of course, any delay of the buffet onset by decreasing or canceling the aerodynamic instabilities would permit to increase flight performances of the aircraft. For example, the aircraft take-off weight, maneuverability, or the range, can be increased.

The aim of this study is to control the buffet phenomenon by a direct action device on the flow instability. As a new moving part at the trailing edge of the wing, a so-called "Trailing Edge Deflector" (TED), designed at ONERA, is used to decrease these instabilities.

This control system study, here limited to two-dimensional flows and to the aerodynamic aspect of the phenomenon, will be further studied in

---

[1] Dept. Models for Aerodynamics and Energetics (DMAE)

[2] Dept. System Control and Flight Dynamics (DCSD)

[3] Dept. Computational Fluid Dynamics and Aeroacoustics (DSNA)

three-dimensional flow [1, 2].

In order to analyze the effect of the new control system on the buffet instabilities and to help for better understanding of the manner in which the deflector can act on flow separations and shock wave oscillations over the airfoil, experimental investigations were performed on the stiff 2D airfoil (OAT15A) in the T2 wind tunnel.

Numerically in addition, the time-consistent strong viscous-inviscid interaction approach VIS15 [3, 4], developed previously for computing buffet or unsteady separated flows over airfoils, was used to give access to a direct time-accurate simulation of the active buffet control with TED servo-command, both in open-loop control, and in the closed-loop servo-command driven by the computed self-induced signals of buffet themselves [5].

2. Model and instrumentation

An experimental investigation on the effects of the deflector on buffet characteristics of an OAT15A airfoil was carried out in T2 wind tunnel of DMAE, a department at ONERA Toulouse (fig:1). T2 is a transonic, pressurized and cryogenic wind tunnel with closed circuit [6]. The test section, equipped with top and bottom flexible walls is $0,37m$ high by $0,39m$ wide and $1,4m$ long. The OAT15A airfoil is a supercritical airfoil designed by ONERA with a thickness-to-chord ratio of $12,6\%$, a chord of $200mm$ and a span of $0,39m$ extending the full width of the tunnel. The model has a design point of $M = 0,73$ and a lift coefficient of $C_l = 0,65$. It is equipped with 60 steady and 19 unsteady pressure transducers. Their locations on the airfoil are shown in figure 2. The signals were sampled at 15kHz with a filter at $5kHz$. All of the tests were performed at a Reynolds number of approximately $Re_c = 4,5.10^6$ with transition fixed at $\frac{x}{c} = 7\%$ on upper and lower sides of the model. The tests were performed at ambient temperature. The Mach number varied between $M_o = 0,72 - 0,78$ and the maximum value of the angle of incidence was $\alpha = 3,5^o$. For the design Mach number of $M_o = 0,73$, the shock wave position moves with a frequency of around $f = 75$ Hz in "buffet" conditions.

• Trailing-edge deflector description

The deflector is situated at the lower surface of the trailing edge (fig:3). It is maintained along the wingspan. Its chord-wise length is only 1 to 3 percent of the airfoil chord. It can be moved from -5° up to 45°, and have a maximum frequency of $200Hz$. For manufacturing problems, it is made of 3 parts. Each of them, simultaneously, are set to the same position or put in motion. It is driven by an electrical mo-

tor. Aerodynamic results of the deflector effects are presented in the next paragraphs.

3. Upper surface buffet description in two-dimensional transonic flow

Buffeting can appear in many flow conditions. In transonic flow, it is accentuated by the shock wave motion.

Natural instabilities on airfoil appear by an increase in the Mach number or the angle of attack. In transonic flow, the buffet is characterized by a complex interaction between shock wave and boundary layer [7, 8]. The shock wave oscillations are caused by flow separation, as shown by the numerical solution VIS15 (fig:4). The buffet onset starts when the separation bubble increases and joins the trailing edge. Then, instabilities develop on a large scale.

The shock-wave moves upstream, pushed by flow separation. Therefore, the flow separation decreases and the shock wave moves back downstream. Thus, the intensity of the shock wave increases and a new separation bubble is created. The flow separation spreads to the trailing edge and push the shock wave upstream again (fig:4).

One of the characteristics of the buffet in two-dimensional flow is that the harmonic spectrum of the shock wave motion exhibits a dominant frequency, plus lower harmonics. This fundamental frequency depends on the shape of the airfoil and on the aerodynamic flow conditions [9, 10].

4. Time-accurate numerical simulation of active buffet control : VIS15 code

The VIS15 numerical method is a "time-consistent strong" Viscous-Inviscid Interaction (VII) approach that was generated a few years ago [3, 4], and that was the first VII method giving the same capability of direct access to a time-accurate simulation of transonic buffet [3, 11, 12] or unsteady separated flows over airfoils [3, 4] as the RANS approaches. More recently, the VIS15 method was extended to the EUROSHOCK passive/active control of buffet through porous walls [13], and to the full time-accurate direct simulation of active buffet control in closed servo-command loop with the present TED device [5], or with the EREA deforming bump device.

The VIS15 code is basically issued from the common methodology of the Viscous-Inviscid Solvers "VIS" developed at ONERA from 1979 [14], using in unsteady equations the same turbulent models and viscous numerical schemes as first designed in steady 2D-3D viscous flows [14, 15, 16, 17], but restricting (in VIS15) the inviscid part of the VIS solver to the transonic small perturbation approximation, while extending the VII strong coupling to a time-consistent one (viscous and inviscid unsteady equa-

tions "discretized and coupled until convergence" at same time-step), so recovering the same domain of influence and same fully time-parabolic nature as the averaged Navier-Stokes RANS equations.

In VIS15, a thin-layer approximation of Le Balleur's "Defect-Formulation theory" [14, 15, 17, 16] for Navier-Stokes equations is used. This theory assumes at all points a splitting of the equations system (RANS Navier-Stokes) in two exactly equivalent strongly interacting equation systems : the viscous "Defect-Formulation" system and the pseudo-inviscid-flow, both of them being solved on the same physical domain. The advantages of this VII approach consist in a very low computational cost that doesn't grow with the Reynolds' number, a much lower undesiderable numerical viscosity, and a high flexibility in choosing at will the viscous approximations level, ranging from boundary-layer to full RANS. At any approximation level, the full overlay of viscous and inviscid computational domains ensures the respect of the full viscous upstream influence in supersonic areas [18], and of a normal pressure gradient inside viscous layers [14, 15, 17, 16].

The thin-layer viscous approximation in VIS15 is assumed in a "displacement-body reference frame" [17, 16], which extends the range of the thin-layer assumption and gives access to "massive separations" and "deep stall".

The viscous numerical method [14, 16, 17, 3] is a field/integral hybrid method, with y-discretization (but with y-rank lower than discretization), that involves a space-marching technique using non-linearly implicit schemes, implicit turbulence coupling, and a switch of direct/inverse modes of solution. It is usable both in steady or unsteady conditions. At each viscous station, "parametric" modeled turbulent velocity profiles [17, 16, 14, 15] — ranging from attached flow to massive separation — are discretized along the direction normal to the local inviscid interacting flow streamlines, on a normal grid that is self-adaptive to the boundary layer thickness and the maximal normal velocity gradient (fig.9).

The method includes first an algebraic turbulence model [14, 15, 17, 16], based on the discretized parametric velocity profiles and on a mixing-length, and secondly an out-of-equilibrium two equation model "$k - u'v'$ forced ", Le Balleur [14, 15, 17, 16], "forced" by the parametric velocity profiles modelling, and selected in all present computations.

For the resolution of the inviscid system, an unsteady transonic small perturbations (TSP) method, extension of [19] with revised schemes, is used in VIS15. The strong coupling is numerically obtained using the original "Semi-Implicit" algorithm defined in 1984 [3, 4], which converges the VII coupling residuals both in direct and inverse viscous modes, after extracting a viscous influence operator, and with an

iterative marching conditioning. The convergence is imposed at each time step in order to obtain a time-consistent strong-coupling method and thus to take into account at each time step the full downstream-upstream viscous influence (as in Navier-Stokes solutions). Doing this enables the proper treatment of strong viscous interaction phenomena in the unsteady case, such as unsteady separations and shock – boundary layer interactions.

5. Comparison of numerical solutions with experiments

5.1. Numerical conditions

Numerical flow conditions are identical to experiments (table 1).

R_{ec}	P_{to}	T_{to}	c	xtr/c
$4,3.10^6$	1.7 bar	300 K	0.2 m	7%

Table 1. Numerical conditions

The VIS15 inviscid grid-part used for calculations is (200 × 100), with a few streamwise refinements at leading-edge, trailing-edge, and in the region of oscillating shock-induced separation. Figure 8 shows a zoom of the inviscid grid. The extent of the computational domain is 10 chord lengths upstream/downstream, and 10 chord lengths upper/lower. The VIS15 overlaying viscous grid-part, figure 9, is made of 2 × (163 × 49) points, has wall nodes in coincidence with the 2 × (163) inviscid nodes along the upper/lower sides of the airfoil and wake-cut, and self-adapts its 49 nodes in normal direction to the local thickness and maximal gradient of the viscous velocity profiles. The VIS15 grid refinement at shock separation is designed, with local streamwise meshes smaller than the boundary layer thickness (ΔX about 0.5δ), in order to effectively discretize and resolve numerically the instantaneous physical extent of compressions at turbulent shock-induced separation.

To allow a good comparison between experiments and calculations, it is important to apply some corrections on the Mach number M_o and on the angle of attack.

T2 wind tunnel is equipped with top and bottom flexible walls. As a result, classical corrections for this two walls aren't necessary, at least at steady flow conditions. However boundary layers that appear on the lateral walls of the wind tunnel induce a flow deceleration. A negative correction of the Mach number is necessary. For T2 wind tunnel, this correction is estimated to $\delta M = -0.06$.

For a good comparison it is essential to compare the same level of buffet. So a correction of the angle of attack is done for the two particular studied

cases : one before the buffet onset and one another beyond buffet onset. Corrections applied to this two cases, which are still not fully optimized (in shock position), are indicated in table 2.

case	Mo_{expe}	Mo_{VIS15}	α_{expe}	α_{VIS15}
1	0.736	0.73	$2.5°$	$2.34°$
2	0.736	0.73	$2.125°$	$2.1°$

Table 2. Studied cases

5.2. Characteristics of OAT15A buffet

The transonic buffet is characterized by pressure fluctuations and oscillations of the shock wave. The figure 5 shows the pressure fluctuations on the airfoil. The unsteady pressure transducers on the oscillation band of the shock wave indicate a high level of fluctuations. Downstream of the shock wave, fluctuations are still important due to flow separation instabilities. Upstream of the shock wave, in the supersonic region, the fluctuations are low.

The numerical VIS15 solution reproduces well the fluctuations behaviour (fig:5), despite an optimal adjustment of the shock mean position is not here achieved, as shown by the zero-harmonic of the pressure (fig:6), which also displays the good prediction of the steep pressure evolution at trailing-edge on lower-side.

The instabilities are mainly-harmonic. Figure 7 illustrates the shock position vs time. The shock wave oscillation frequency is about $f = 75Hz$ in experiment, whereas a somewhat lower frequency (increasing with angle of attack from about $f = 53Hz$ for incipient buffet to $f = 60Hz$ for well established buffet) is computed by VIS15. It is not yet fully clear whether this numerical shift in fundamental frequency is due to the TSP inviscid truncation still used in the case of VIS15, or to the form of the TSP variant used [19], or to the free-air solution.

More informations on buffet measurements are given in references [20, 21, 22].

5.3. Effects of a static TED change

The trailing edge deflector can be moved to a particular position. Before buffet onset, increasing static TED defection acts on shock wave position and on flow separation levels. The supersonic level is increased and the shock wave moves downstream. Also, the trailing edge thickness is increased and the flow is modified in this region (fig:10). All these effects are well detected by VIS15 numerical calculations (fig:11).

The buffet onset can be detected by the pressure fluctuation levels. The lift coefficient can be determined by pressure integration. The figure 12 shows the buffet onset. The angle of attack of the buffet onset is well detected by the VIS15 solution, where however the buffet onset is somewhat more brutal than in the experimental results. The figures 12 and 13 indicate the effects of two positions of the deflector ($\delta = 0°$ and $\delta = 15°$) on the buffet onset. The incidence of buffet onset is decreased with a deflector angle increase, but the lift at buffet onset is increased. Both effects are well predicted numerically by VIS15.

The calculations overestimate slightly the lift coefficient because of their downstream shock-wave position. The figure 13 indicates the steady lift coefficient vs the angle of attack for the two positions of the deflector ($\delta = 0°$ and $\delta = 15°$). At iso-incidence, an increased deflector angle increases the lift coefficient for the airfoil.

The figure14 represents the buffet onset by means of the fluctuation amplitude of a local pressure coefficient ($x/c = 0.9$). Experimentally, the pressure fluctuations are calculated for two frequency bands $[5 - 4000Hz]$ and $[50 - 100Hz]$. This allows to know the difference between the separation flow noise and the buffet phenomenon. VIS15 calculations give a buffet onset that is very close to experimental buffet onset in the $[50 - 100Hz]$ frequency band. As a result, it seems that the buffet phenomenon is well modelized by VIS15. An important effect of the deflector is to delay the buffet onset at iso Mach-Cz. The figure 14 illustrates this benefit displayed by experiments, and well reproduced by VIS15 calculations.

The drag polar clearly shows the increase in aerodynamic performances for high lift coefficient (fig:15), but, for lower lift coefficient, there is no profit. VIS15 gives the same results (fig:15).

5.4. Open loop control - Effects of a dynamic TED motion

The deflector can be driven by dynamic movements around a static position. Different deflector motions were tested to try to understand the effects of the deflector motion on natural buffet (fig:16).

• Step motion of TED

Deflector step motions were tested. This kind of motion is very interesting because it allows to study and understand the crossing mechanisms from a flow state to another one. Different cases were studied. The figure 17 shows the buffet onset by variation of the deflector angle. This figure indicates the extremal upstream and downstream positions of the

shock-wave. The shock-wave oscillation starts more brutally by VIS15 calculations than by experiments. However, the comparison is very good.

An interesting case is the switch from a steady state to a buffet state. The figure 18 indicates the shock-wave oscillations for a step from $\delta = 5^o$ to $\delta = 25^o$. VIS15 can visualize the whole flow field. The figure 19 shows the propagation in time of the Mach number perturbation which is created by the step at the time $t = 0ms$. The perturbation takes about $1ms$ to go upstream in the subsonic region of the upper surface and to reach the shock wave. It seems to be an acoustic propagation. On the lower surface of the airfoil, the perturbation takes about $2ms$ to go to the upper surface. It's also an acoustic propagation. The perturbation goes round the leading edge and in the supersonic region. The required time to reach the shock wave is about $1ms$. It is not a simple acoustic propagation. Presently, we don't know how to explain it.

● **Sine-shaped TED motions at steady flow conditions**

Firstly, sine-shaped signals prescribed to the deflector motion were tested at steady flow conditions. Figure 20 shows the shock wave amplitude oscillations for different frequencies of the deflector (experimental results). The deflector motion creates shock wave oscillations. The amplitude of the shock wave oscillations and its frequency depend on the deflector motion. The deflector motion creates shock wave oscillations at the same frequency than the deflector. This hanging up of frequency is observed for all frequencies of the deflector. The higher the amplitude of the deflector is, the greater the amplitude of the shock wave oscillations will be. The amplitude of the shock wave oscillations varies with the frequency of the deflector. The highest amplitude of the shock wave oscillation is observed for a frequency of the deflector which is near the natural buffet frequency. All this remarks are well predicted by numerical VIS15 calculations in figure 21. Except for an amplitude deflector of $A = \pm 10^o$, the greater amplitude of the shock wave oscillation is observed for a frequency of the deflector which is lower than the computed natural buffet frequency.

● **Sine-shaped TED motion at natural buffet flow conditions**

At flow conditions with natural buffet, the motion of the deflector can, for certain amplitudes and frequencies, impose its frequency to shock wave and flow separations oscillations. The higher the amplitude of the deflector is, the greater the influence field will be. The figure 22 illustrates the domain of influence in frequency for 3 amplitudes ($A = \pm 2.5^o$;

$A = \pm 5^o$; $A = \pm 10^o$) by calculations and experiments.

VIS15 calculation solutions give a slightly greater domain of influence than experiments, but behaviours are identical.

For deflector motion frequencies far from the natural buffet frequency, the shock wave keeps its natural frequency, but the amplitude of oscillations are modulated by the deflector motion.

Experimentally, the amplitude of the deflector $A = \pm 2.5^o$ have just few effects on the shock wave oscillations while calculation solutions give more effects. In experiments, the real position of the deflector was measured by a camera [20]. For little amplitudes ordered, the real deflector amplitude is lower than the commanded amplitude. For $A = \pm 2.5^o$, we find a real amplitude about $A = \pm 1.0^o$ [21]. For the amplitudes ordered of $A = \pm 5^o$ and $A = \pm 10^o$, the real deflector amplitude are near the commanded amplitudes. Experimental and numerical behaviours are comparable. For these amplitudes, the deflector motion causes an increase in shock wave oscillations.

5.5. Closed loop command - Active buffet control

Some phase shifts of sine-shaped open loop motions of the TED (deflector angle phase vs. shock position phase) have permitted a brief stabilization of the unsteady buffeting flow. But, it's impossible to control the buffet phenomenon only by this kind of motion. If an open loop command allows to understand the effects of a deflector motion, a closed loop of servocommand is required to stabilize the shock wave oscillations. It is based on the unsteady measurements of pressure fluctuations (fig:25). We saw in the previous sections that a decrease in the deflector angle involves an upstream motion of the shock-wave, and an increase in the deflector angle involves a downstream shock wave motion. So, the idea is to move the deflector in order that it is acting against the natural shock wave movement.

The control law for a measured signal P is described by:

$$\delta(t) = \delta_{mean} + \delta^{'}(t), \tag{1}$$

with,

$$\delta^{'}(t) = A * (P(t - \tau) - P_{mean}), \tag{2}$$

Different control laws were tested based on the same principle. Different measured signals can be used for control : pressure fluctuations taken on a transducer which is located on the shock wave oscillations region, or shock-wave position, or lift. The same signals were also enabled to drive the control law when this one was introduced in VIS15 [5]. The control law's parameters (A, τ) weren't determined a priori. Different gains A and time delays τ were looked for. We can find an optimal couple that depends on

the conditions and the chosen driving signal. Different couples (A and τ) were tested both by the experiments, and by the numerical VIS15 calculations in closed-loop self-command. Experiments as well VIS15 calculations showed [5] that a pressure signal coming from the rear part of the shock wave oscillating region is the most efficient choice with the present control law, due to it's persistent amplitude (i.e. the pressure jump through shock wave).

By using for the command signal the unsteady measurements of pressure fluctuations, the buffet and the shock wave oscillations were greatly reduced in experiment (fig. 26 and 27). By using the same control principle, the buffet can be completely reduced (fig:28) in the numerical VIS15 simulation. Calculations are less expensive than experiments. Then, different new laws will be tested by calculations in order to find new control laws for three-dimensional flow.

6. Conclusion

The experimental study has shown the efficiency of a trailing edge deflector on two-dimensional flow. The TED can be moved to a particular position or be driven by dynamic motions. A selected static position increases aerodynamic performances for high lift coefficient and delays the buffet onset. An active control law driven by unsteady measurements allows to greatly reduce the aerodynamic instabilities.

Numerical solutions obtained by the time-consistent viscous-inviscid strong interaction code VIS15 are in a whole accordance with experiments. The self-command within VIS15 computation of the deflector, driven in closed-loop by the computed buffet pressure signals themselves, provides very good results for time-accurate direct numerical simulation of the active buffet control. Numerical results allow to help to better understand the phenomena and to give a second validation of efficiency of the TED. Different new laws will be tested by calculations in order to find new control laws which could be used in three-dimensional buffet.

This new control system will soon be studied in transonic three-dimensional flow. A similar model extended to a transport aircraft was designed and manufactured with TED. Experimental tests are planned in 2000.

References

[1] D. Caruana, M. Corrège, O. Reberga, C. Despré, and A. Mignosi. Buffet and buffeting active control. *AIAA Fluids 2000 - Flow Control Symposium*, AIAA paper(2000-2609), 19-22 June 2000.

[2] C. Despré. Analyse de quelques résultats expérimentaux des essais DYVAS en vue de la préparation et de l'étude de la demi-voilure OAT15A-CA. Technical report ONERA n° RT12/00866 DPRS/DMAE, ONERA, Mars 2000.

[3] J.C. Le Balleur and P. Girodroux-Lavigne. A semi-implicit and unsteady numerical method of viscous-inviscid interaction for transonic separated flows. *La Recherche Aérospatiale 1984-1, p.15-37, English and French editions*, Jan. 1984.

[4] J.C. Le Balleur and P. Girodroux-Lavigne. A viscous-inviscid interaction method for computing unsteady transonic separation. *Proceed. 3rd Symp. "Numerical and Physical Aspects of Aerodynamic flows", Long-Beach, USA, January 21-24, 1985), T. Cebeci ed., Springer-verlag 1987, or ONERA TP 1985-5.*

[5] H. Gassot, P. Girodroux-Lavigne, and J.C. Le Balleur. Simulation numérique instationnaire VIS15 du contrôle actif du tremblement transsonique bidimensionnel : actionneur de bord de fuite. *RT 4/6207 DPRS/N/DSNA, Mars 1999.*

[6] A. Séraudie J.P. Archambaud. The Cryogenic Induction Tunnel T2 at Toulouse. *AGARD FDP/VKI Special Course*, May 1996.

[7] N.C. Lambourne. Some instabilities arising from the interactions between shock waves and boundary layers. Technical Report, Advisory Group for Aeronautical Research and development. Report 182., April 1958.

[8] J.M. Délery. Shock wave/turbulent boundary layer interaction and its control. *Prog. Aerospace Sci.*, 22:209-280, 1985.

[9] B. Benoît. Etude du champ de pression instationnaire sur le profil RA16SC1 en régime de tremblement à S3MA. Technical Report, Rapport technique de synthèse ONERA, June 1986.

[10] B.H.K. Lee. Effects of trailing-edge flap on buffet characteristics of a supercritical airfoil. *Journal of Aircraft*, 29(1), January-February 1992.

[11] J.C. Le Balleur and P. Girodroux-Lavigne. Prediction of buffeting and calculation of unsteady boundary layer separation over airfoils. *Proceed. IUTAM Symp. "boundary layer separation", London, August 26-28, 1986, p. 19-35, editor F.T. Smith, S.N. Brown, Springer-Verlag 1987, or ONERA TP 1986-95.*

[12] J.C. Le Balleur and P. Girodroux-Lavigne. Viscous-Inviscid Strategy and Computation of transonic Buffet. *Proceed. Symp. IUTAM Transsonicum III, Gottingen, May 24-27, 1988, Springer-Verlag 1988, or ONERA TP 1988-111.*

[13] J.C. Le Balleur, P. Girodroux-Lavigne, and H. Gassot. Development of Viscous-Inviscid Interaction Codes for Prediction of Shock Boundary Layer Interaction Control (SBLIC) and Buffet over Airfoils. *Brite-Euram EUROSHOCK - Drag Reduction by Passive Shock Control. Notes on Numeri-*

cal Fluid Mechanics, Vol. 56, Chap. 15, pp. 221-244, Vieweg 1997.

[14] J.C. Le Balleur. Strong matching method for computing transonic viscous flows including wakes and separations. Lifting airfoils. *La Recherche Aérospatiale 1981-3, p.21-45, English and French editions,* May 1981.

[15] J.C. Le Balleur. Numerical viscous-inviscid interaction in steady and unsteady flows. *Proceed. 2nd Symp. "Numerical and Physical Aspects of Aerodynamic flows", Long-Beach, (1983), chap. 13, p. 259-284, T. Cebeci ed., Springer-verlag, (1984), (or ONERA TP 1983-8).*

[16] J.C. Le Balleur. New possibilities of viscous-inviscid numerical techniques for solving viscous flow equations, with massive separation. *Proceed. Fourth Symp. Numerical-Physical Aspects of Aero. flows, Long-Beach, USA, Jan. 16-19, 1989, Selected papers, chap. 4, p. 71-96, Cebeci ed., Springer-verlag, 1990. (or ONERA TP 1989-24).*

[17] J.C. Le Balleur. Viscous-inviscid calculation of high-lift separated compressible flows over airfoils and wings. *Proceedings AGARD-CP-515, paper 26, Symposium AGARD/FDP "High-lift aerodynamics", Banff, Canada, 5-8 octobre 1992, (or ONERA TP 1992-184).*

[18] J.C. Le Balleur. Viscous-inviscid flow matching : Analysis of the problem including separation and shock waves. *La Recherche Aérospatiale 1977-6, p.349-358, French, or English transl.ESA-TT-476,* Nov. 1977.

[19] M. Couston, J. J. Angelini, and P. Mulak. Application de l'équation de petites perturbations transsoniques aux calculs d'écoulements bidimentionnels instationnaires. *La Recherche Aérospatiale 1979-5, p. 325-341, (Sept 1979),* Sept. 1979.

[20] D. Caruana, M. Corrège, O. Reberga, J.B. Dor, and C. Lempereur. Contrôle actif des instabilités aérodynamiques à l'origine du tremblement. Ecoulement transsonique bidimenssionnel. Phase 1. Technical Report, ONERA, Décembre 1998.

[21] D. Caruana, M. Corrège, O. Reberga, J.B. Dor, C. Despré, and J.F. Breil. Contrôle actif des instabilités aérodynamiques à l'origine du tremblement. Ecoulement transsonique bidimenssionnel. Phase 2. Technical Report, ONERA, Juin 1999.

[22] O. Reberga. *Etude expérimentale et numérique du phénomène de tremblement sur profil d'aile et son contrôle en écoulement transsonique avec onde de choc.* PhD thesis, ENSAE, June 2000.

7. Figures
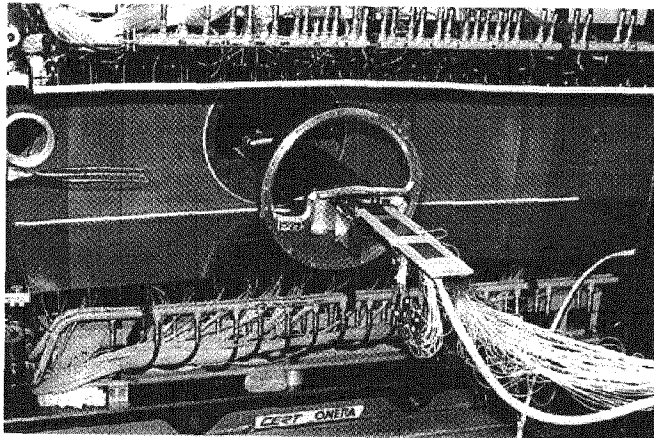
Figure 1. T2 transonic wind tunnel with OAT15A airfoil

Pressure transducers { + steady
                       o unsteady
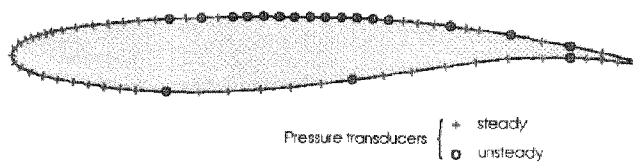
Figure 2. Model instrumentation
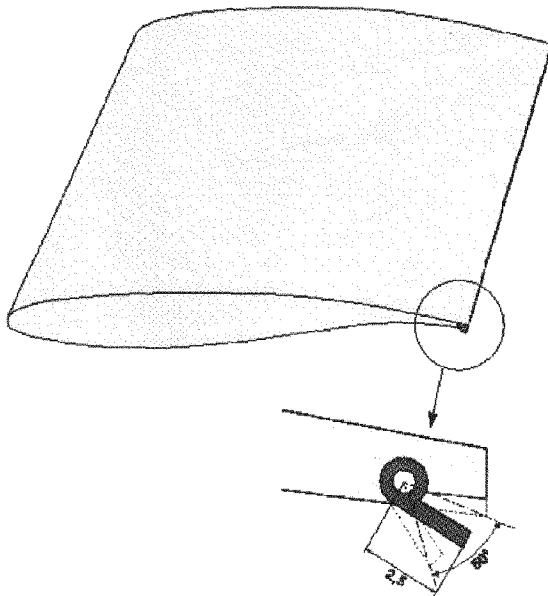
Figure 3. Trailing edge deflector
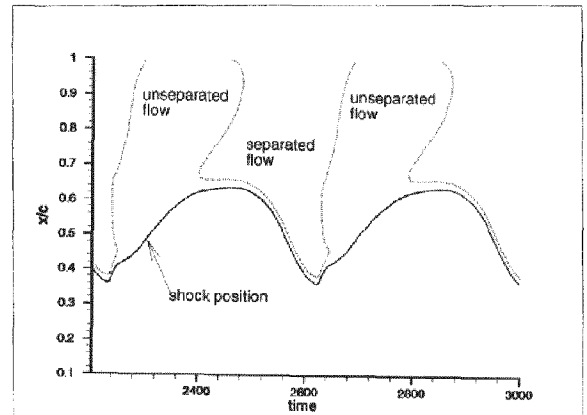
Figure 4. Flow separation areas with the shock position in buffet conditions (Numerical VIS15 solution)
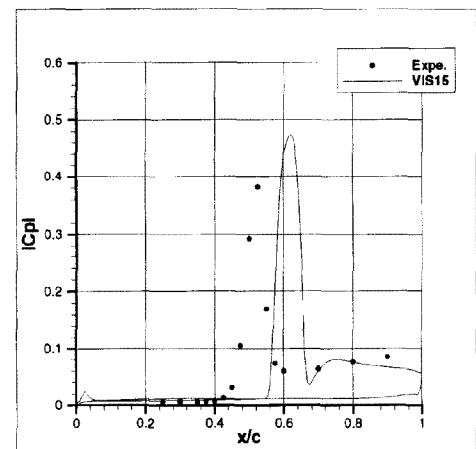
Figure 5. Pressure fluctuations on airfoil - Comparisons of numerical VIS15 solution (M=0.73; $\alpha = 2.34°$; $\delta = 15°$) with experiments (M=0.736; $\alpha = 2.5°$; $\delta = 15°$)
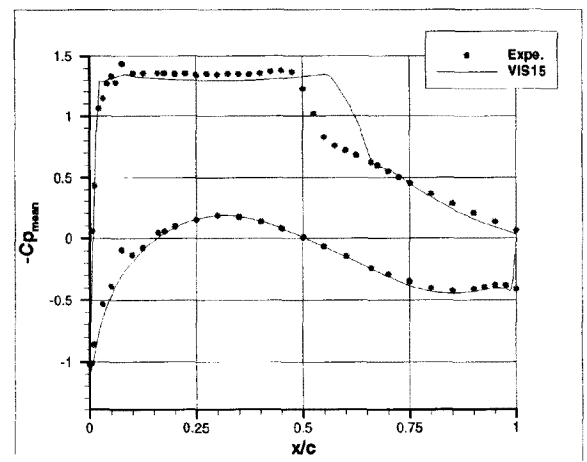
Figure 6. Zero-harmonic of the pressure coefficient - Comparisons of numerical VIS15 solution (M=0.73; $\alpha = 2.34°$; $\delta = 15°$) with experiments (M=0.736; $\alpha = 2.5°$; $\delta = 15°$)
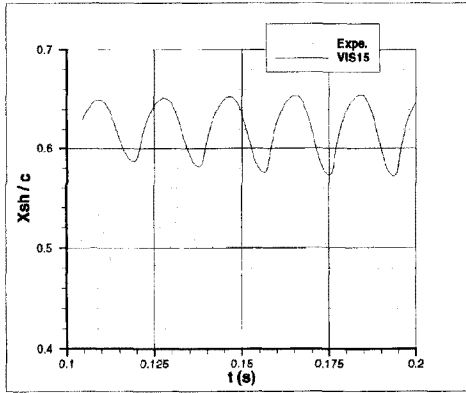
Figure 7. Shock wave position on the airfoil vs time - Comparisons of numerical VIS15 solution (M=0.73; $\alpha = 2.34°$; $\delta = 15°$) with experiments (M=0.736; $\alpha = 2.5°$; $\delta = 15°$)
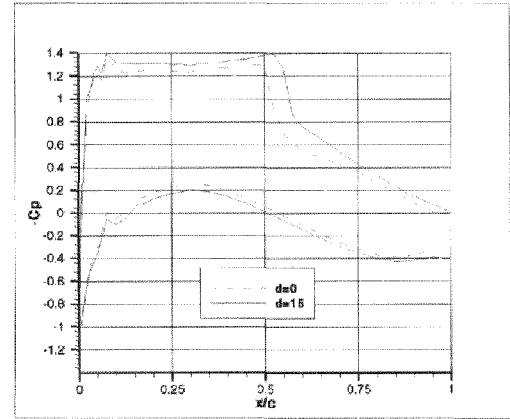
Figure 10. Effects of the static deflector position - Experimental Results (M=0.736; $\alpha = 2.0$; $\delta = 0°$; $\delta = 15°$)
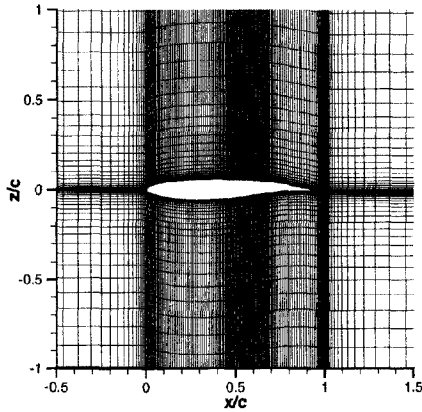
Figure 8. Inviscid part of VIS15 mesh - Zoom on partial view
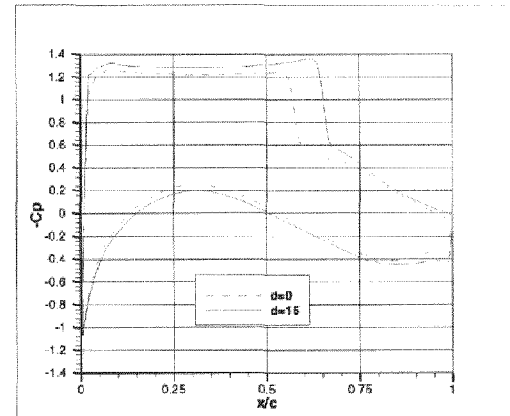
Figure 11. Effects of the static deflector position - Numerical VIS15 solutions (M=0.73; $\alpha = 2.0$; $\delta = 0°$; $\delta = 15°$)
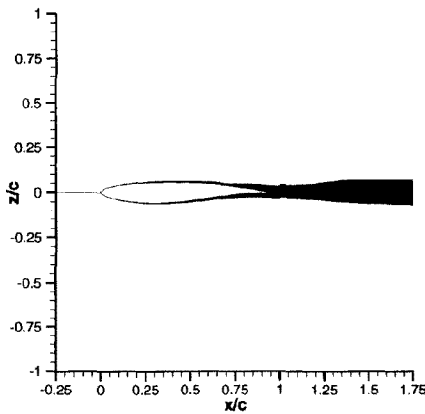
Figure 9. Viscous part of VIS15 mesh - Zoom on partial view
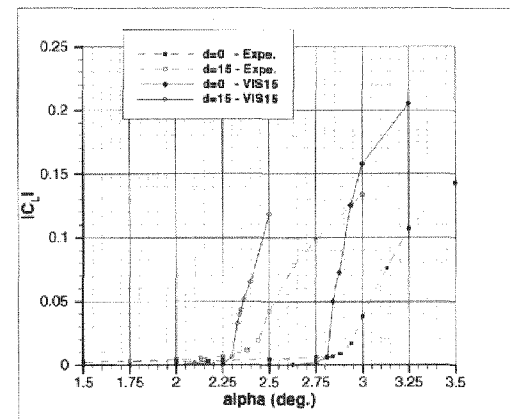
Figure 12. Variation of the fluctuations of lift coefficient with the angle of attack - Comparisons of numerical VIS15 solutions with experiments
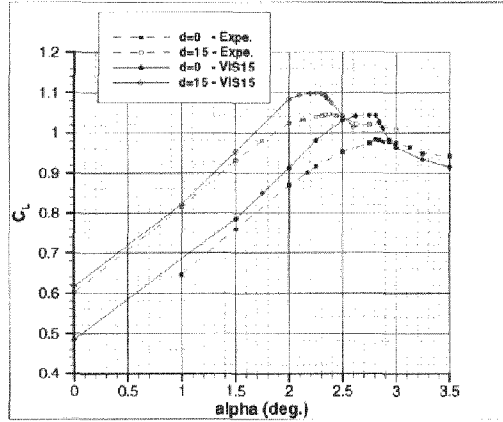
Figure 13. Variation of lift coefficient with the angle of attack - Comparisons of numerical VIS15 solutions with experiments
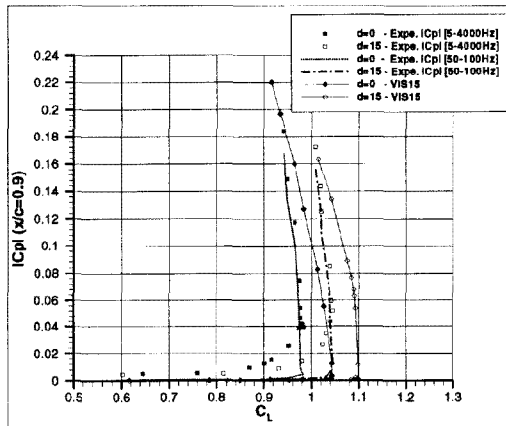
Figure 14. Buffet onset - Pressure fluctuations x/c=0.9 - Comparisons of numerical VIS15 solutions with experiments
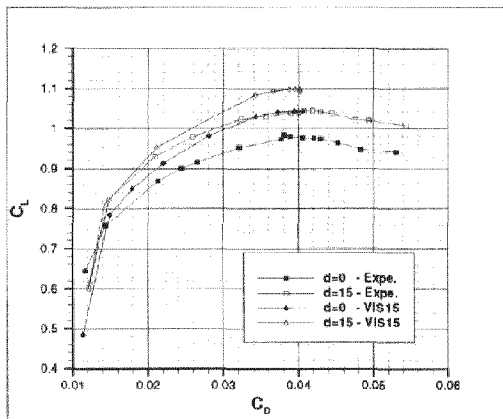
Figure 15. Drag polar - Comparisons of numerical VIS15 solutions with experiments
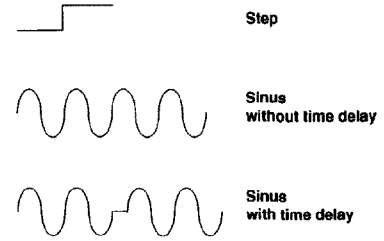
Figure 16. Different motions of the deflector
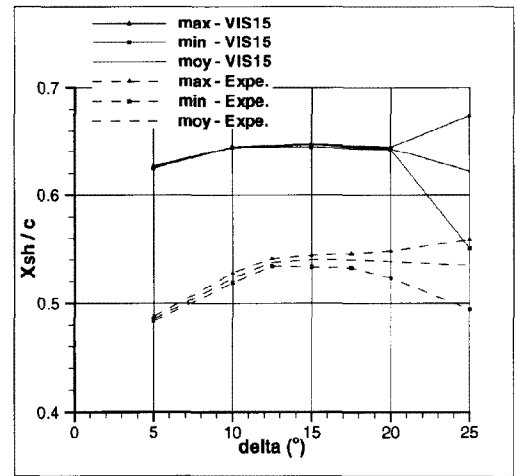
Figure 17. Variation of the extremal shock positions with the angle of the deflector - Comparisons of numerical VIS15 solutions (M=0.73; α = 2.1) with experiments (M=0.736; α = 2.13)
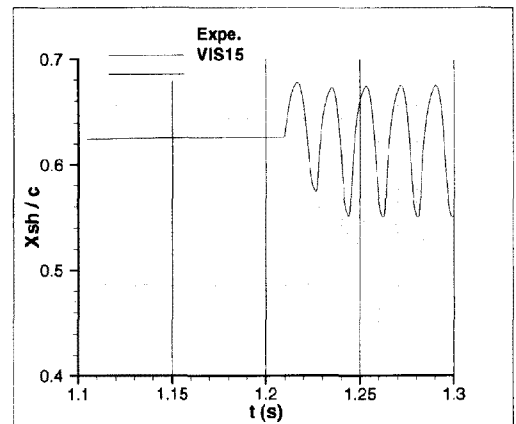
Figure 18. Variation of the shock position vs time after a step of deflector angle from $\delta = 5^{o}$ to $\delta = 25^{o}$ - Comparisons of numerical VIS15 solution (M=0.73; α = 2.1) with experiments (M=0.736; α = 2.13)
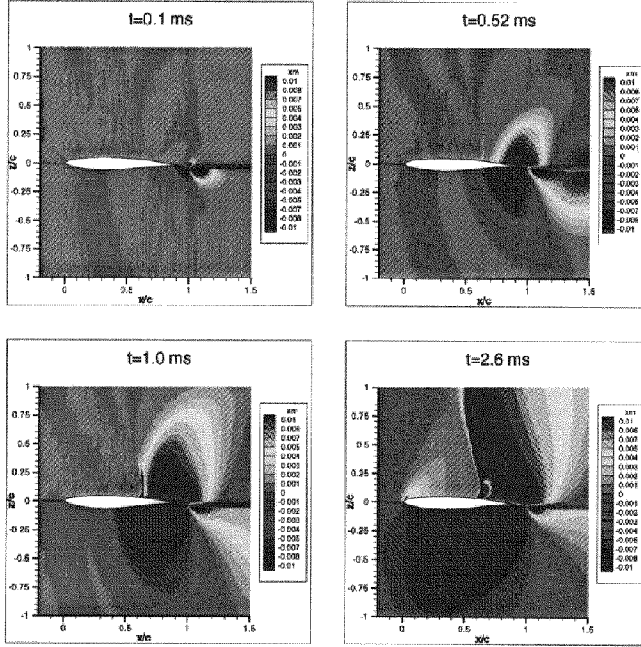
Figure 19. Propagation of the perturbation of Mach number generated after a step of deflector angle from $\delta = 5^{\circ}$ to $\delta = 25^{\circ}$ at a time $t = 0ms$ - Numerical VIS15 solution (M=0.73; $\alpha = 2.1$)
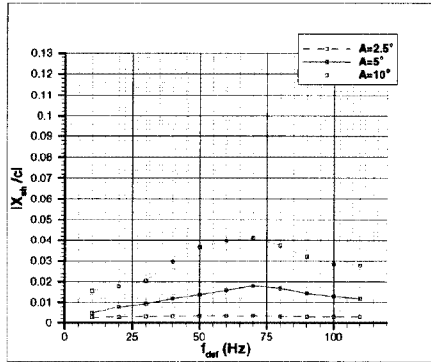

Figure 22. Frequency domain of influence on buffet of the deflector motion vs deflector amplitude - Comparisons of numerical VIS15 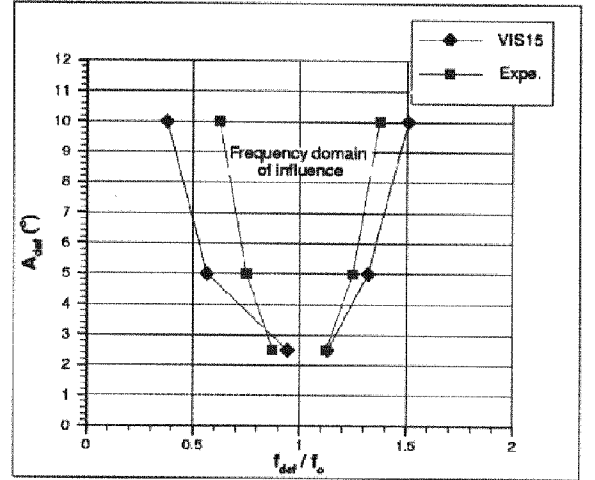solutions (M=0.73; $\alpha = 2.34$; $d_{mean} = 15^{\circ}$) with experiments (M=0.736; $\alpha = 2.5$; $d_{mean} = 15^{\circ}$)

Figure 20. Effects of sine-shaped deflector motion before the buffet onset - Shock fluctuations vs deflector frequency at 3 amplitudes - Experimental results (M=0.736; $\alpha = 2.13$; $d_{mean} = 15^{\circ}$)
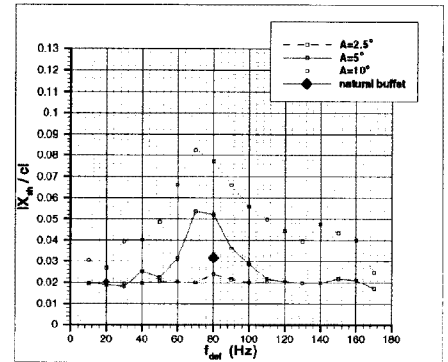

Figure 23. Effects of sine-shaped deflector motion at natural buffet conditions - Shock fluctuations vs frequency at 3 amplitudes - Experimental results (M=0.736; $\alpha = 2.5$; $d_{mean} = 15^{\circ}$)

Figure 21. Effects of sine-shaped deflector motion before the buffet onset - Skock fluctuations vs deflector frequency at 3 amplitudes - Numerical VIS15 results (M=0.73; $\alpha = 2.1$; $d_{mean} = 15^{\circ}$)
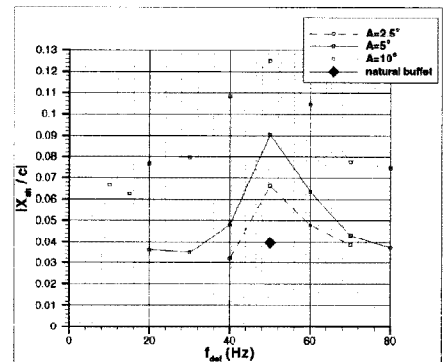

Figure 24. Effects of sine-shaped deflector motion at natural buffet conditions - Shock fluctuations vs frequency at 3 amplitudes - Numerical VIS15 results (M=0.73; $\alpha = 2.34$; $d_{mean} = 15^{\circ}$)
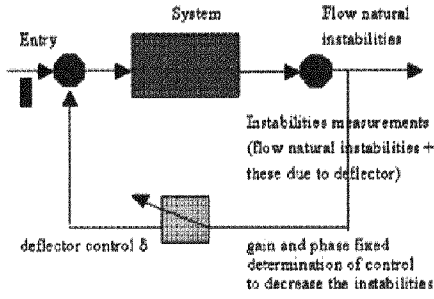
Figure 25. Principle of the active control law - Closed-loop active buffet control
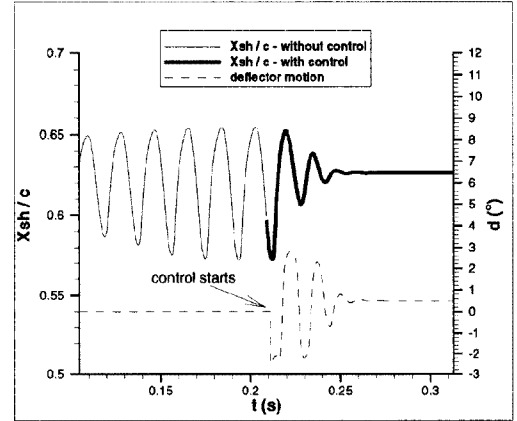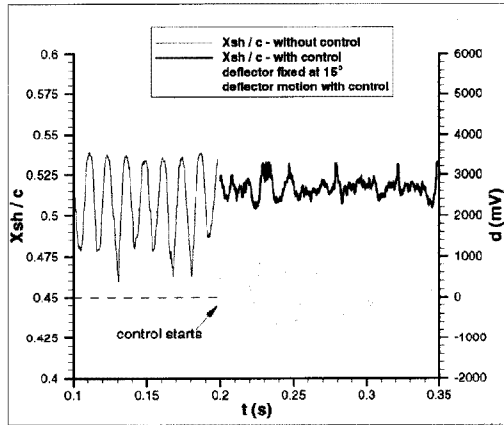

Figure 26. Effects of a closed-loop active buffet control on the shock position - Experimental results (M=0.736; $\alpha = 2.5^o$; $d_{mean} = 15^o$; Control law: $A = 5$; $\phi = 90^o$; $Cp(\frac{x}{c} = 0.525)$)
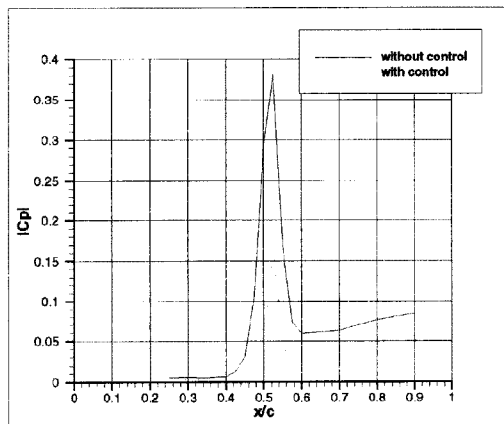

Figure 27. Effects of a closed-loop active buffet control on pressure fluctuations on the airfoil - Experimental results (M=0.736; $\alpha = 2.5^o$; $d_{mean} = 15^o$; Control law: $A = 5$; $\phi = 30^o$; $Cp(\frac{x}{c} = 0.525)$)

Figure 28. Effects of a closed-loop active buffet control on the shock position - Direct numerical VIS15 simulation (M=0.73; $\alpha = 2.34^o$; $d_{mean} = 15^o$; Control law: $A = 3$; $\phi = 45^o$; $Cp(\frac{x}{c} = 0.63)$)

Paper #15

Q by Dr. Bram Elsenaar: Is the preferred frequency of 75Hz related to a preferred structural mode of the model, like bending ? If yes, is this represented in the theoretical model; or can you explain the difference in frequency (50Hz in theory)

A. (Despre): No the model can be considered as stiff (2-D model spanning the walls). We don't have an explanation for this difference; it may be related to the difference in shock position, or maybe it is due to the TSP inviscid truncation still used in the case of VlS15, or to the form of TSP variant used.

This page has been deliberately left blank

———————————

Page intentionnellement blanche